Conversely, the present technique is hampered by neither of these issues (*14*).

The excellent agreement between theoretically and experimentally determined rate constants for reaction 1 presented here validates these methods and should permit the measurement of rate constants for a wide range of atom-radical reactions in the near future. It is envisaged that reactions of ground-state atomic nitrogen and oxygen with other small diatomic radicals (CN, CH, C_2) will be among the first to be investigated. Our results also bear on the discrepancies between observed N/N_2 abundance ratios and those predicted by current astrochemical models. Maret *et al*. (*6*) used parameters given by the Ohio State University astrochemical database (OSU 2005) (*23*) to obtain rate constants for reactions 1 and 2 in their chemical model of the B68 prestellar core. At 10 K, these parameters yield rate constants of 1.4×10^{-10} $cm^3\ s^{-1}$ and 2.3×10^{-10} $cm^3\ s^{-1}$ for reactions 1 and 2, respectively. The present results can be used to estimate a rate constant for reaction 1 of 2.5×10^{-11} $cm^3\ s^{-1}$ at 10 K. Similarly, from recent experimental (*5*) and theoretical studies (*24*, *25*) of reaction 2, we estimate a rate constant of 7×10^{-12} $cm^3\ s^{-1}$. With values 5 and 30 times smaller than those used in the model example (*6*), this gas-phase N_2 formation mechanism should be less important than previously thought.

References and Notes

1. E. Herbst, H.-H. Lee, D. A. Howe, T. J. Millar, *Mon. Not. R. Astron. Soc.* **268**, 335 (1994).
2. CRESU stands for Cinétique de Reaction en Ecoulement Supersonique Uniforme and was applied to the study of reactions between neutral species by Sims *et al*. (*26*).
3. C. Berteloite *et al*., *Phys. Rev. Lett.* **105**, 203201 (2010).
4. D. Carty, A. Goddard, S. P. K. Köhler, I. R. Sims, I. W. M. Smith, *J. Phys. Chem. A* **110**, 3101 (2006).
5. A. Bergeat, K. M. Hickson, N. Daugey, P. Caubet, M. Costes, *Phys. Chem. Chem. Phys.* **11**, 8149 (2009).
6. S. Maret, E. A. Bergin, C. J. Lada, *Nature* **442**, 425 (2006).
7. J. Woodall, M. Agúndez, A. J. Markwick-Kemper, T. J. Millar, *Astron. Astrophys.* **466**, 1197 (2007).
8. V. Wakelam *et al*., *Space Sci. Rev.* **156**, 13 (2010).
9. I. W. M. Smith, D. W. A. Stewart, *J. Chem. Soc. Faraday Trans.* **90**, 3221 (1994).
10. D. Edvardsson, C. F. Williams, D. C. Clary, *Chem. Phys. Lett.* **431**, 261 (2006).
11. M. Jorfi, P. Honvault, P. Halvick, *Chem. Phys. Lett.* **471**, 65 (2009).
12. A. Li, C. Xie, D. Xie, H. Guo, *J. Chem. Phys.* **134**, 194309 (2011).
13. J. Daranlot *et al*., *ChemPhysChem* **11**, 4002 (2010).
14. Materials and methods are detailed in the supporting material at *Science* Online.
15. P. Honvault, J.-M. Launay, in *Theory of Chemical Reaction Dynamics*, A. Lagana, G. Lendvay, Eds. (Kluwer, Dordrecht, Netherlands, 2004), pp. 187–215.
16. J. M. Bowman, *J. Phys. Chem.* **95**, 4960 (1991).
17. Z. Sun, H. Guo, D. H. Zhang, *J. Chem. Phys.* **132**, 084112 (2010).
18. M. M. Graff, A. F. J. Wagner, *J. Chem. Phys.* **92**, 2423 (1990).
19. M.-H. Ge, T.-S. Chu, K.-L. Han, *J. Theor. Comput. Chem.* **7**, 607 (2008).
20. F. Lique *et al*., *J. Chem. Phys.* **131**, 221104 (2009).
21. W. H. Brune, J. J. Schwab, J. G. Anderson, *J. Phys. Chem.* **87**, 4503 (1983).
22. M. J. Howard, I. W. M. Smith, *J. Chem. Soc. Faraday Trans. II* **77**, 997 (1981).
23. E. Herbst, Ohio State University Astrochemical Database (update OSU.2005); www.physics.ohio-state.edu/~eric/research_files/osu.2005.
24. M. Jorfi, P. Honvault, *J. Phys. Chem. A* **113**, 10648 (2009).
25. P. Gamallo, R. Martínez, R. Sayós, M. González, *J. Chem. Phys.* **132**, 144304 (2010).
26. I. R. Sims *et al*., *J. Chem. Phys.* **97**, 8798 (1992).

Acknowledgments: Our experimental work was supported by the Agence Nationale de la Recherche (grant ANR-JC08_311018), the Conseil Régional d'Aquitaine (grant 20091102002), and the European Union (grant PERG03-GA-2008-230805). Our theoretical work was supported by the Mésocentre de Calcul de Franche-Comté (M.J. and P.H.), the U.S. Department of Energy (H.G.) and the National Natural Science Foundation of China (grants 21133006, 91021010, and 20725312) (D.X.). The data described in this work can be obtained from the corresponding author on request.

Supporting Online Material

www.sciencemag.org/cgi/content/full/334/6062/1538/DC1
Materials and Methods
Table S1
References (*27*–*44*)

9 September 2011; accepted 19 October 2011
10.1126/science.1213789

Observing the Multiexciton State in Singlet Fission and Ensuing Ultrafast Multielectron Transfer

Wai-Lun Chan, Manuel Ligges, Askat Jailaubekov, Loren Kaake, Luis Miaja-Avila, X.-Y. Zhu*

Multiple exciton generation (MEG) refers to the creation of two or more electron-hole pairs from the absorption of one photon. Although MEG holds great promise, it has proven challenging to implement, and questions remain about the underlying photo-physical dynamics in nanocrystalline as well as molecular media. Using the model system of pentacene/fullerene bilayers and femtosecond nonlinear spectroscopies, we directly observed the multiexciton (ME) state ensuing from singlet fission (a molecular manifestation of MEG) in pentacene. The data suggest that the state exists in coherent superposition with the singlet populated by optical excitation. We also found that multiple electron transfer from the ME state to the fullerene occurs on a subpicosecond time scale, which is one order of magnitude faster than that from the triplet exciton state.

The absorption of one photon in most semiconductor materials creates one electron-hole pair, which may be separated to give electrical current in a photovoltaic device. The solar-to-electric power-conversion efficiency from such a device comprising a single semiconductor material is theoretically limited to ~31%. This value, referred to as the Shockley-Queisser (SQ) limit (*1*), comes about because any excess kinetic energy of electron-hole pairs excited by photons with energy above the bandgap is typically lost as waste heat. One viable approach to exceed the SQ limit is to use materials in which the excess energy from the absorption of one photon can create two or more electron-hole pairs in a process called multiple exciton generation (MEG), or carrier multiplication in inorganic semiconductors (*2*, *3*) and singlet fission (SF) in the more localized molecules (*4*). MEG has been observed in semiconductor nanocrystals (*5*–*8*) and single-walled carbon nanotubes (*9*) and has been predicted to occur efficiently in graphene (*10*). SF in organic molecules is also well established (*4*) and can approach quantum efficiencies as high as 200% (*11*).

Implementing MEG or SF in high-efficiency solar cells requires extraction of multiple electrons or holes from the light-harvesting material. This is challenging because in competition with charge extraction, there are a number of competing channels for the decay of multiple excitons. For example, enhanced Coulomb interaction (*12*) is believed to be responsible for high MEG yield in quantum-confined materials but also increases the efficiency of Auger recombination (the reverse of MEG). Charge-carrier extraction from multiple excitons has been demonstrated with the assistance of external bias voltage in photodiodes of single-walled carbon nanotubes (*9*), PbS nanocrystal thin films (*13*), and pentacene/C_{60} multilayers (*14*). Multiple charge transfer has also been reported for molecular electron acceptors anchored to semiconductor nanocrystals (*15*) and in semiconductor nanocrystal-sensitized electrochemical solar cells (*16*).

In the above demonstrations and in extensive ongoing efforts, the common strategy has been to extract charge carriers from the product of the MEG or SF process, that is, relaxed (band-edge) or localized multiple excitons. However, this approach may not be the best strategy to harvest carriers resulting from MEG. Theoretical studies of SF in molecular materials have shown that the process involves a multiexciton (ME) intermediate state, which is essentially a correlated triplet

Department of Chemistry and Biochemistry, University of Texas, Austin, TX 78712, USA.

*To whom correspondence should be addressed. E-mail: zhu@cm.utexas.edu

exciton pair $^1(TT)$ with an overall singlet spin multiplicity (*4*, *17*):

$$S_0 + S_1 \rightleftharpoons {}^1(TT) \rightleftharpoons T_1 + T_1 \qquad (1)$$

In the following, we will use ME in place of $^1(TT)$ for simplicity. The first step in Eq. 1 has traditionally been viewed as a kinetic process that occurs on ultrafast time scales. In the second step, decoherence and relaxation of the ME state lead to two individual triplets. If multiple electrons or holes can be extracted on ultrafast time scales directly from the ME state, carrier extraction might be more likely to out-compete Auger recombination. Efficient carrier extraction from the ME state would also shift the balance between the strongly coupled single exciton and the ME state, thus increasing the yield of MEG in return (*18*).

We chose the pentacene/C_{60} bilayer as a model system because pentacene is known to possess a high singlet-to-triplet fission rate (*4*). The dissociation of triplet excitons at the donor/acceptor interface is believed to be responsible for the ~145% quantum efficiency in a pentacene/C_{60} multilayer photodetector (*14*) and for the near-unity internal quantum efficiency of pentacene/C_{60} bilayer thin-film solar cells (*19*, *20*). The lowest-energy singlet exciton (S_1) transition energy in crystalline pentacene is 1.83 eV, which is more than twice the triplet (T_1) energy (2 × 0.86 = 1.72 eV) (*4*, *20*). This makes SF an energetically favorable process. Previous studies on excition fission dynamics in pentacene have relied on transient absorption spectroscopy (*4*, *20*–*24*). There are considerable disagreements on the details of spectroscopic assignments because of spectral overlap and the unknown optical transition frequencies. Although there is a consensus on the S_1 exciton decay time of 70 to 100 fs, the reported rise times for the T_1 state range from ~80 fs (*21*, *24*) to 1 ps (*22*, *23*). Recent theoretical studies (*25*, *26*) reported a ME intermediate state for SF in pentacene, but there has been little experimental information on this state. We used femtosecond time-resolved two-photon photoemission (TR-2PPE) spectroscopy to show that the ME state in pentacene is in fact the predominant species immediately produced by optical excitation—a result of a coherent quantum mechanical resonance between the S_1 and the ME state. Moreover, direct multiple-electron extraction from the ME state is not only possible but also a rapid channel for electron transfer.

We prepared the samples by means of vapor deposition in an ultrahigh vacuum environment. We first grew an epitaxial C_{60} thin film on a single crystal Au (111) surface and then deposited pentacene on the C_{60} surface. Pentacene is known to form a bulk-like crystalline phase on the C_{60} surface, with the long molecular axis aligned close to the surface normal (*27*). In TR-2PPE measurements, the electrons were excited by a visible pump laser pulse ($h\nu_1$ = 2.15 eV) and ionized by a time-delayed ultraviolet (UV) probe laser pulse ($h\nu_2$ = 4.65 eV). The photoelectrons were detected with a hemispherical electron energy analyzer. The TR-2PPE technique allows us to track the complete time evolution of the fission process, as illustrated in Fig. 1A. TR-2PPE spectra from a sample with 10 monolayers (ML; 1 ML = 1.5 nm) of pentacene are shown in Fig. 1B. Representative spectra at three different pump-probe delays (vertical cuts) are shown in Fig. 1C. The initial excitation creates a short-lived peak at E_k = 1.34 eV, corresponding to a transiently populated state at 3.31 eV below the vacuum level (E_{vac}). We assign this peak as originating from the S_1 state because this position, along with the optical band gap of 1.83 eV, gives the highest occupied molecular orbital (HOMO) at 5.14 eV below E_{vac}, which is in agreement with UV photoemission measurements (*28*). At longer delay times, the spectrum is dominated by one peak at E_k = 0.38 eV, which remains nearly constant in energy for as long as 300 ps after initial excitation (fig. S3). This long-lived peak is at 0.96 ± 0.05 eV below S_1 and is assigned to the T_1 state.

We now discuss a particular observation in Fig. 1: the peak labeled ME that is slightly higher in energy than the triplet at early times (< 1 ps) but merges into the triplet at longer times. This peak cannot be formed from the incoherent decay of S_1. As shown in Fig. 1D, the S_1 peak rises within the optical pulse rise time and decays with a time constant of τ_{S1} = 110 ± 20 fs (Fig. 1D, green squares). The ME peak (Fig. 1D, black circles) rises concurrently with S_1 because of optical excitation but clearly does not stem from the decay of S_1 (Fig. 1D, blue curve; prediction from a rate equation based on τ_{S1}). Because direct optical excitation to T_1 is forbidden, this peak cannot be the ordinary triplet. We conclude that this peak signifies the elusive ME state as proposed in various theoretical models in the past (*4*, *25*, *26*). Contrary to common invocation of an incoherent rate process for S_1-to-ME conversion (Eq. 1), the concurrent formation of these two states indicates that the initial optical excitation creates a superposition of S_1 and ME because of strong electronic coupling between the two, as proposed in

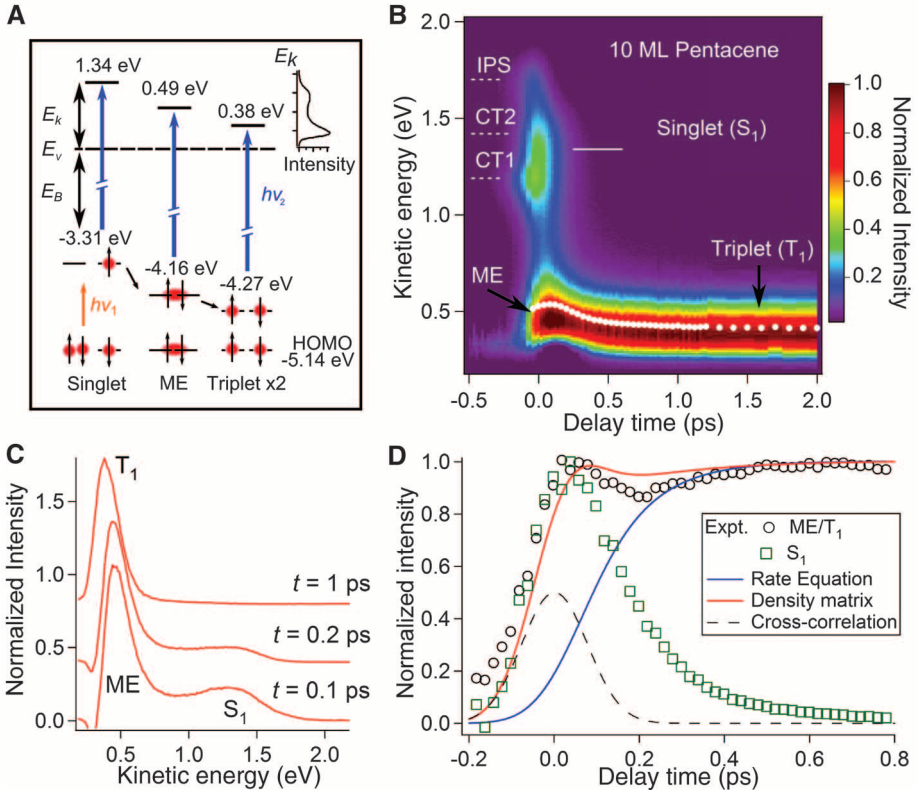

Fig. 1. (**A**) Illustration of the detection of singlet, ME, and two triplets states in pentacence by TR-2PPE ($h\nu_1$ = 2.15 eV; $h\nu_2$ = 4.65 eV). (**B**) Pseudo-color representation of TR-2PPE spectra for a 10-ML pentacene sample. The positive delay time with visible-pump and UV-probe shows photoemission from the transiently formed S_1, the ME, and the T_1 states. The negative time corresponds to UV (4.65 eV) pump and visible (2.15 eV) probe and shows features due to the image potential state (IPS) and charge-transfer excitons (CT1 and CT2) on the surface of pentacene (SOM text). The white circles are electron energy (center of gravity) of the ME/T_1 spectral feature as a function of pump-probe delay. (**C**) Vertical cuts (spectra) of the two-dimensional plot in (B) at the indicated pump-probe delays. (**D**) The population of the S_1 state (open squares) and the total population of the ME/T_1 states (open circles) as a function of pump-probe delay at early times. For the S_1 population, contribution from CT excitons at negative time delays has been subtracted (SOM text). The dashed curve is the expected cross correlation of the pump-probe laser pulses assuming Gaussian pulse shapes with experimentally determined pulse widths. The blue curve is the simulated ME/T_1 population from the rate equation with a formation time constant of τ = 110 fs. The red curve is simulated by using optical Bloch equations in the coherent superposition model (SOM text).

theoretical studies of MEG in semiconductor nanocrystals (*18*) and SF in organics (*29*).

The absorption of one photon can initially only generate a single electron-hole pair. Because the ME state consists of two correlated electron-hole pairs—that is, $^1(TT)$—it is optically dark (*18*, *25*). Within the coherent superposition model, S_1 is populated by the laser field, whereas the dark ME state is populated indirectly via electronic coupling to S_1. This process can be modeled in a density matrix formulism (*18*, *29*), and the result [detailed in the supporting online material (SOM) text] is shown as the red curve in Fig. 1D for the ME population. To account for the nearly instantaneous rise in S_1 and ME populations, we found that the electronic coupling constant (W) between S_1 and ME must be larger than 50 meV, given the putative difference in the rise times of less than 20 fs, which is the time resolution resulting from 100-fs laser pulses; the modeling result in Fig. 1D is based on W = 330 meV. The model can reproduce quantitatively the ultrashort S_1 lifetime (τ_{S1} = 110 ± 20 fs) because of decoupling of ME from S_1 by electronic decoherence (fig. S4) and also qualitatively a small dip in ME population at a time approximately coinciding with the decrease in the optical field before a rise again at longer times (≥200 fs). The latter can be explained by the coherent and indirect coupling between ME and S_0 through S_1 by the optical field.

The strong electronic coupling is between a dark ME state and a bright S_1 state. This coupling has no effect on the ME yield, as clarified previously in the theoretical work of Shabaev, Efros, and Nozik (*18*) and also detailed in the SOM text. In the density matrix formulism, the initial optical excitation only accesses the S_1 state (*18*, *29*), and the system evolves with time because of coupling to ME. The SF yield depends on the relative rates of decay/relaxation from the ME and S_1 states (Eq. 3), independent of photon energy (within the S_1 manifold), as verified experimentally (fig. S7). Strong electronic coupling is expected to result in coherent oscillation between the ME and S_1 populations, but the large electronic coupling constant (>50 meV) corresponds to an ultrashort oscillation time period not resolvable in our experiments owing to the relative long laser pulse width (~100 fs) used. For comparison, coherent oscillation of the superposition state can be observed in the time domain for weaker electronic coupling, as discovered recently in photosynthetic pigment-protein complexes (*30*–*32*). The electronic coupling between S_1 and ME (W > 50 meV) may also lead to a splitting of the S_0–S_1 transition under CW light excitation. This may be partially responsible for the broad and complex absorption spectrum of solid pentacene (*33*).

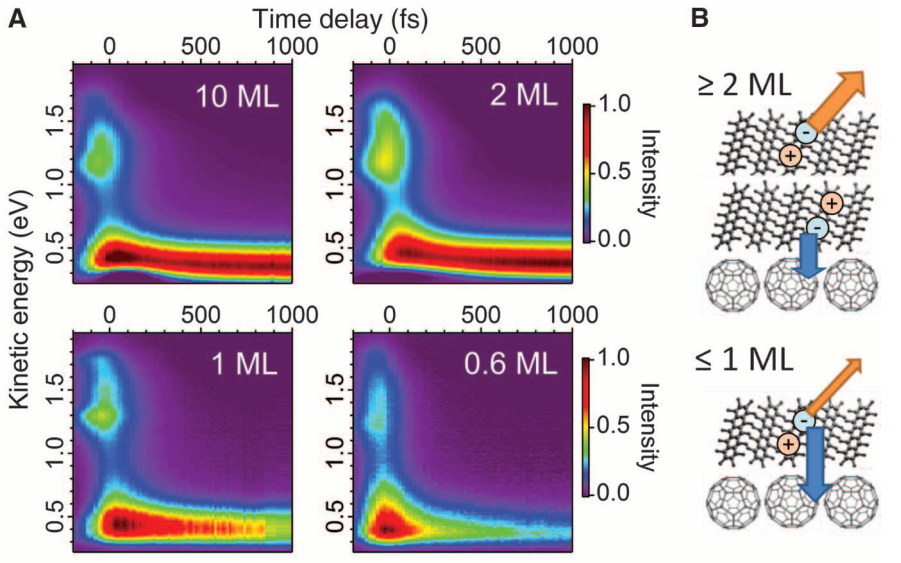

Fig. 2. (**A**) Pseudo-color representation of TR-2PPE spectra for pentacene thin films of 10, 2, 1, and 0.6 ML thickness deposited on crystalline C_{60}. (**B**) Schematic illustrations of photoemission (orange arrows) and charge transfer to C_{60} (blue arrows). The TR-2PPE technique is only sensitive to photoemission from the topmost layer, whereas charge transfer only occurs in the bottommost layer of the pentacene thin film.

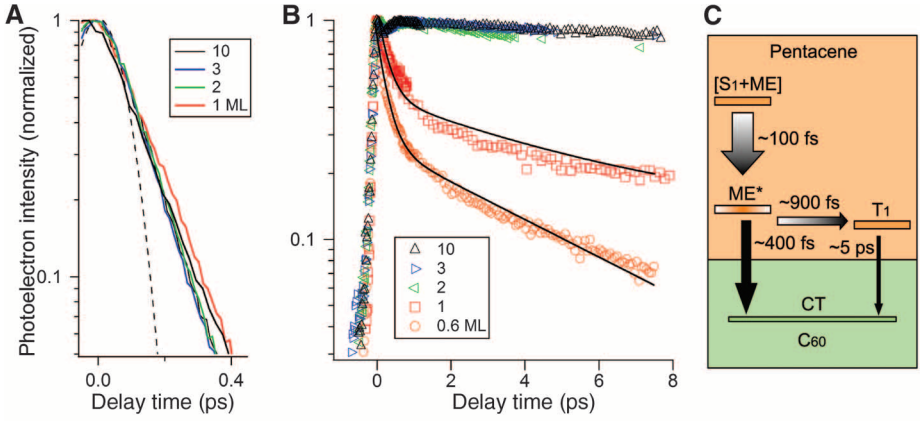

Fig. 3. (**A**) Singlet decay dynamics of pentacene films with thicknesses of 10, 3, 2, and 1 ML deposited on crystalline C_{60}. The dashed line represents the cross-correlation of the laser pulses. (**B**) ME/T_1 decay dynamics of 10, 3, 2, 1, and 0.6 ML pentacene films. The solid lines represent fits to the kinetic model described in the SOM text. (**C**) Summary of exciton decay and charge-transfer dynamics at the pentacene/C_{60} interface.

The nature of the ME state is revealed by the energetic relaxation process, which merges the ME into the triplets in <1 ps. Near time (t) zero, the mean kinetic energy of the ME state (Fig. 1B, open circles) is 0.11 ± 0.01 eV higher in energy than that of T_1 at longer times. This energy difference is identical to the total exothermicity ($\Delta E = 1.83 - 2 \times 0.86 = 0.11$ eV). Thus, S_1 and ME are energetically resonant at t = 0; photoelectrons from these two states emerge at different kinetic energies because photoionization of S_1 (by $h\nu_2$) leaves a hole in the HOMO as a final product, whereas photoionization of ME leaves a hole in the HOMO plus a T_1 state behind. The sensitivity of 2PPE to this distinction is a major advantage of the technique. The irreversible energetic relaxation of ME, which is well described by a time constant of τ_E = 260 ± 50 fs (fig. S2), is probably the main reason for dephasing and decoupling between ME and S_1. The photoelectron intensity arising from the ME is similar to that from the two triplet states. This is not surprising because ME is essentially a correlated triplet pair and can be a source of two excited electrons.

On the basis of the above results, the traditional rate equation model in Eq. 1 for singlet fission is revised to Eq. 2,

$$[S_1 \Leftrightarrow \mathrm{ME}] \rightarrow \mathrm{ME}' \rightarrow T_1 + T_1 \qquad (2)$$

where the initial optical excitation creates the $[S_1 \Leftrightarrow \mathrm{ME}]$ superposition; the first step in Eq. 2 describes electronic dephasing to yield ME states (ME′) that are no longer coupled to S_1, and the second step describes relaxation/localization of the ME state to two individual triplets. Both steps are dynamic processes involving a continuum of configurations. A strict distinction between ME′ and $2T_1$ is difficult and unnecessary because it depends on one's definition of correlation between

two triplets. Steps 2 and 3 in Eq. 2 can also be reversible in general.

Having established the mechanism of exciton fission in pentacene, we next turned to electron transfer from the excitonic states to the electron acceptor C_{60}. We probed the electron transfer dynamics by varying the thickness of pentacene deposited on C_{60}. For pentacene coverage in the multilayer region (2 to 10 ML), the 2PPE spectra do not change appreciably with coverage (Fig. 2A): The technique probes mainly the topmost layer owing to a finite electron escape depth, and the exciton dynamics in thicker pentacene films are insensitive to the presence of C_{60}. The situation is very different in the monolayer/submonolayer region, where the pentacene layer probed by 2PPE is in direct contact with C_{60}. The ME/ME′ and T_1 populations are quenched rapidly, presumably because of charge transfer to C_{60} (*14*, *20*).

Quantitative analysis of data in Fig. 2 gives relative excitonic state populations (photoemission intensities) as a function of pump-probe delay (Fig. 3). For the S_1 state (Fig. 3A), we found that the population decays with a single exponential lifetime of $\tau_{S1} = 110 \pm 20$ fs, independent of film thickness. We conclude that singlet decay is dominated by dephasing and relaxation of the ME state; electron transfer from the S_1 state to C_{60} is evidently not competitive on such a short time scale. The ME population (Fig. 3B) rises instantaneously, and there are population dips due to the optical coherence effect discussed above (details of early time dynamics are in fig. S5). The ME state evolves to ME′ and $2T_1$ at $t > 100$ fs. Thereafter, the total ME/ME′/$2T_1$ population remains nearly constant for films with pentacene thickness of ≥2 ML. In these samples, the triplet in the topmost layer decays on a much longer time scale of ~250 to 350 ps (fig. S9). For sub-monolayer (0.6 ML) and 1-ML coverage, the total ME/T_1 population decays with two time constants: an initial fast sub-picosecond component and a slower component of a few picoseconds. The switching between these two regimes corresponds to the time scale when the ME relaxes into two triplets.

The transient population can be reproduced by a simple kinetic model shown in Fig. 3C (SOM text). The model allows direct charge transfer from the ME/ME′ to C_{60}. The ME′ can relax into a pair of T_1, which can also participate in charge transfer with a different rate constant. Furthermore, the data for 1-ML film show a small constant offset from the 0.6-ML curve at longer delay times (>1 ps). Prior studies have shown that small islands of a second molecular layer start to form on top of an incomplete first molecular layer when the coverage of the first layer is ≥0.8 ML (*34*). Therefore, for 1-ML pentacene an additional term with a time constant of 250 ps is included. Our fitting shows that this term accounts for ~13% of the photoemission intensity. We optimized the fit for the 1 ML and 0.6 ML data using the same set of time constants. The solid curve shows the result. The time constants of electron transfer from ME to C_{60} is $\tau_{ME} = 400 \pm 100$ fs, whereas that from T_1 to C_{60} is $\tau_{T1} = 5 \pm 1$ ps. The time constant for the transformation from ME′ to T_1 from the kinetic fit is $\tau_{ME \rightarrow T1} = 900 \pm 300$ fs, which is in agreement with the 1-ps rise time of triplet observed in some transient absorption studies (22,23). The ~85-fs rise time reported in the most recent transient absorption study by Wilson *et al*. (*24*) probably corresponds to the formation of ME′.

We highlight two findings from the kinetic analysis. First, the rate constant of electron transfer to C_{60} from the ME/ME′ states ($1/\tau_{ME} = 2.5 \pm 0.6 \times 10^{12}$ s^{-1}) is more than one order of magnitude higher than that from T_1 ($1/\tau_{T1} = 2.0 \pm 0.4 \times 10^{11}$ s^{-1}). This surprising observation may be qualitatively understood. At early times in the dynamic process, the wave function of the excited state (ME/ME′) is more diffuse or delocalized in crystalline pentacene and thus may possess stronger electronic coupling to C_{60}, leading to ultrafast electron transfer in the strong electronic coupling region. The second finding is that both excited electrons in the ME state must be transferred. As detailed in the SOM text and fig. S6, a hypothetical model assuming the transfer of only one electron from ME/ME′—resulting in one hole and a T_1 state in pentacene—is incompatible with experimental data. An alternative hypothesis is that there is only one electron transfer to C_{60} from the ME/ME′ state in pentacene, but the resulting T_1 state undergoes prompt nonradiative recombination because of the presence of the hole. If this hypothesis were true, the quantum efficiency for interfacial electron transfer could not be much higher than 100%. This would contradict the findings of Baldo and co-workers, who reported 145% external quantum efficiency for photocurrent generation in a pentacene/C_{60} multilayer photodetector (*14*). Because the photodetector consisted of alternating pentacene and C_{60} layers, each with monolayer thickness, direct interfacial charge separation instead of exciton transport must dominate photocurrent generation. Considering other optical and electrical losses, the quantum efficiency for interfacial electron transfer is probably higher than 145%.

To further quantify the charge-transfer dynamics, we used a complementary technique—time-resolved second harmonic generation (TR-SHG) (*35*)—to probe the transient electric field established by exciton dissociation and charge-transfer across the interface. The approach is a four-wave mixing process in which two optical fields of frequency ω mix with the transient charge separation field to give a resultant signal at a frequency ~2ω (Fig. 4, inset). The transient change in SHG intensity ($\Delta I^{2\omega}$) is proportional to the electric field at the interface and hence the number of electrons transferred. The sample we used in the TR-SHG experiments was prepared by spin-coating ~10 nm of a soluble form of fullerene, phenyl-C61-butyric acid methyl ester (PCBM), on an optically flat Al_2O_3 substrate. We chose spin-coating of PCBM over thermal sublimation of C_{60} because the former gives a flat surface (roughness ≤ 1 nm), whereas the latter yields three-dimensional clusters on Al_2O_3. An atomically smooth interface over a large area is critical to the SHG measurement of a transient interfacial electric field. Then, we thermally evaporated 2 ML of pentacene onto the fullerene surface. A TR-SHG measurement (Fig. 4, blue) performed with pump and probe photon energies of 2.00 and 1.65 eV, respectively, is shown in Fig. 4. We see a rapid rise in $\Delta I^{2\omega}$ or interfacial electric field upon excitation of pentacene with a sub-picosecond time constant. This is followed by a small and slow rise of SHG signal, with a time constant of a few picoseconds. For comparison, we show the TR-2PPE signal (Fig. 4, red, inverted axis on right) from the ME/T_1 states for 1 ML of pentacene on C_{60}. Within experimental uncertainty, the rise in electric field at the pentacene/fullerene interface probed by TR-SHG is in excellent agreement with the temporal behavior in the decay in ME/T_1 population observed in TR-2PPE. The one-to-one correspondence of the TR-2PPE and TR-SHG data unambiguously establishes that the decay in ME/T_1 population corresponds quantitatively to electron transfer from pentacene to the C_{60} molecules. Here, the slow rise (a few picoseconds) in interfacial electric field is due to two-electron transfer from two T_1 states, whereas the rapid rise (sub-picosecond) is due to two-electron transfer from the ME/ME′ states.

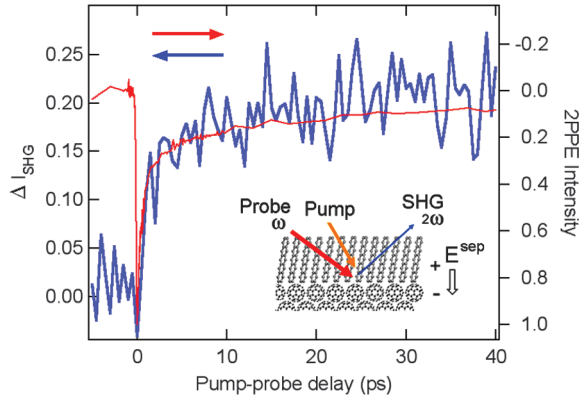

Fig. 4. SHG intensity (blue, left axis) as a function of pump-probe delay time from a sample with 2-ML pentacene deposited on a fullerene (PCBM) thin film. (**Inset**) Schematic illustration of the TR-SHG experiment. The TR-SHG signal probes the transient electric field, E^{sep}, established by charge transfer at the interface. Also shown is normalized 2PPE intensity (red, right axis with inverted scale, reproduced from Fig. 3) of the ME/T_1 state population as a function of delay time for 1-ML pentacene on C_{60}. The 1 ML data are shown here because the 2PPE technique cannot probe interfacial electron transfer when thicker pentacene overlayers are present.

An attractive consequence of charge transfer from the ME states is that it may increase the effective MEG yield. Consider the quantum resonance in Eq. 2. Shabaev *et al.* (*18*) showed that when there are other relaxation channels that can move the two states out of resonance with each other, the effective MEG yield is given by Eq. 3:

$$\frac{N_{ME}}{N_{S_1}} = P_{1\rightarrow 2}\frac{\gamma_2}{\gamma_1} \quad (3)$$

where N_{S_1} is the population of the single exciton state; N_{ME} is the total population of MEs and multiple excitons (including those that have successfully undergone multiple electron transfer); $P_{1\rightarrow 2}$ is the probability of forming the ME from the single exciton; and γ_2 and γ_1 are overall relaxation rates from the ME and the single exciton, respectively. Here, γ_1 can include energy relaxation (cooling) of the initial exciton, radiative or nonradiative recombination channels, and (in the case of pentacene) decay into charge transfer excitons (*33*); γ_2 accounts for energy relaxation or localization to form two triplets here or to form band-edge excitons in nanomaterials. When the additional channel of direct and ultrafast multiple charge transfer from the ME states opens, the total γ_2 increases. This effectively shifts the equilibrium to the ME state and increases the MEG yield, which is akin to Le Châtelier's principle for chemical equilibrium.

The discoveries of the coherent superposition of singlet and ME states and associated ultrafast electron transfer from the ME states in pentacene suggest a distinct design principle in solar energy conversion: the harvesting of multiple charge carriers from the ME state. Such an approach may minimize competing Auger recombination processes and maximize MEG yield.

References and Notes

1. W. Shockley, H. J. Queisser, *J. Appl. Phys.* **32**, 510 (1961).
2. M. C. Hanna, A. J. Nozik, *J. Appl. Phys.* **100**, 074510 (2006).
3. V. I. Klimov, *Appl. Phys. Lett.* **89**, 123118 (2006).
4. M. B. Smith, J. Michl, *Chem. Rev.* **110**, 6891 (2010).
5. J. A. McGuire, J. Joo, J. M. Pietryga, R. D. Schaller, V. I. Klimov, *Acc. Chem. Res.* **41**, 1810 (2008).
6. M. C. Beard *et al.*, *Nano Lett.* **10**, 3019 (2010).
7. M. Ben-Lulu, D. Mocatta, M. Bonn, U. Banin, S. Ruhman, *Nano Lett.* **8**, 1207 (2008).
8. G. Nair, S. M. Geyer, L.-Y. Chang, M. G. Bawendi, *Phys. Rev. B* **78**, 125325 (2008).
9. N. M. Gabor, Z. Zhong, K. Bosnick, J. Park, P. L. McEuen, *Science* **325**, 1367 (2009).
10. T. Winzer, A. Knorr, E. Malic, *Nano Lett.* **10**, 4839 (2010).
11. J. C. Johnson, A. J. Nozik, J. Michl, *J. Am. Chem. Soc.* **132**, 16302 (2010).
12. L. Brus, *Nano Lett.* **10**, 363 (2010).
13. V. Sukhovatkin, S. Hinds, L. Brzozowski, E. H. Sargent, *Science* **324**, 1542 (2009).
14. J. Lee, P. Jadhav, M. A. Baldo, *Appl. Phys. Lett.* **95**, 033301 (2009).
15. J. Huang, Z. Huang, Y. Yang, H. Zhu, T. Lian, *J. Am. Chem. Soc.* **132**, 4858 (2010).
16. J. B. Sambur, T. Novet, B. A. Parkinson, *Science* **330**, 63 (2010).
17. R. C. Johnson, R. E. Merrifield, *Phys. Rev. B* **1**, 896 (1970).
18. A. Shabaev, A. L. Efros, A. J. Nozik, *Nano Lett.* **6**, 2856 (2006).
19. S. Yoo, B. Domercq, B. Kippelen, *Appl. Phys. Lett.* **85**, 5427 (2004).
20. A. Rao *et al.*, *J. Am. Chem. Soc.* **132**, 12698 (2010).
21. C. Jundt *et al.*, *Chem. Phys. Lett.* **241**, 84 (1995).
22. H. Marciniak, I. Pugliesi, B. Nickel, S. Lochbrunner, *Phys. Rev. B* **79**, 235318 (2009).
23. V. K. Thorsmølle *et al.*, *Phys. Rev. Lett.* **102**, 017401 (2009).
24. M. W. B. Wilson *et al.*, *J. Am. Chem. Soc.* **133**, 11830 (2011).
25. P. M. Zimmerman, Z. Zhang, C. B. Musgrave, *Nat. Chem.* **2**, 648 (2010).
26. T. S. Kuhlman, J. Kongsted, K. V. Mikkelsen, K. B. Møller, T. I. Sølling, *J. Am. Chem. Soc.* **132**, 3431 (2010).
27. D. B. Dougherty, W. Jin, W. G. Cullen, J. E. Reutt-Robey, S. W. Robey, *Appl. Phys. Lett.* **94**, 023103 (2009).
28. H. Kakuta *et al.*, *Phys. Rev. Lett.* **98**, 247601 (2007).
29. E. C. Greyson, J. Vura-Weis, J. Michl, M. A. Ratner, *J. Phys. Chem. B* **114**, 14168 (2010).
30. G. S. Engel *et al.*, *Nature* **446**, 782 (2007).
31. G. Panitchayangkoon *et al.*, *Proc. Natl. Acad. Sci. U.S.A.* **107**, 12766 (2010).
32. E. Collini *et al.*, *Nature* **463**, 644 (2010).
33. H. Yamagata *et al.*, *J. Chem. Phys.* **134**, 204703 (2011).
34. F.-J. Meyer zu Heringdorf, M. C. Reuter, R. M. Tromp, *Nature* **412**, 517 (2001).
35. W. A. Tisdale *et al.*, *Science* **328**, 1543 (2010).

Ackowledgments: This work was supported by the National Science Foundation under grant DMR-0804583. The SHG results presented in Fig. 4 were based on work supported as part of the program "Center for Re-Defining Photovoltaic Efficiency Through Molecule Scale Control," an Energy Frontier Research Center funded by the U.S. Department of Energy (DOE), Office of Science, Office of Basic Energy Sciences under award DE-SC0001085. Development of the SHG technique used for Fig. 4 was supported as part of the program "Understanding Charge Separation and Transfer at Interfaces in Energy Materials (EFRC:CST)", an Energy Frontier Research Center funded by the DOE, Office of Science, Office of Basic Energy Sciences under award DE-SC0001091. M.L. acknowledges financial support through SFB616 and the Leopoldina Fellowship Program LPDS 2009-41. X.-Y.Z. acknowledges fruitful discussions with R. E. Wyatt, F. Spano, A. Shabaev, and A. L. Efros.

Supporting Online Material

www.sciencemag.org/cgi/content/full/334/6062/1541/DC1
Materials and Methods
SOM Text
Figs. S1 to S9
References (*36*–*44*)

14 September 2011; accepted 26 October 2011
10.1126/science.1213986

A Coherent Signature of Anthropogenic Nitrogen Deposition to Remote Watersheds of the Northern Hemisphere

Gordon W. Holtgrieve,[1]* Daniel E. Schindler,[1] William O. Hobbs,[2] Peter R. Leavitt,[3] Eric J. Ward,[4] Lynda Bunting,[3] Guangjie Chen,[5,6] Bruce P. Finney,[7] Irene Gregory-Eaves,[5] Sofia Holmgren,[8] Mark J. Lisac,[9] Peter J. Lisi,[1] Koren Nydick,[10] Lauren A. Rogers,[1] Jasmine E. Saros,[11] Daniel T. Selbie,[12] Mark D. Shapley,[7] Patrick B. Walsh,[9] Alexander P. Wolfe[13]

Humans have more than doubled the amount of reactive nitrogen (Nr) added to the biosphere, yet most of what is known about its accumulation and ecological effects is derived from studies of heavily populated regions. Nitrogen (N) stable isotope ratios (^{15}N:^{14}N) in dated sediments from 25 remote Northern Hemisphere lakes show a coherent signal of an isotopically distinct source of N to ecosystems beginning in 1895 ± 10 years (±1 standard deviation). Initial shifts in N isotope composition recorded in lake sediments coincide with anthropogenic CO_2 emissions but accelerate with widespread industrial Nr production during the past half century. Although current atmospheric Nr deposition rates in remote regions are relatively low, anthropogenic N has probably influenced watershed N budgets across the Northern Hemisphere for over a century.

Anthropogenic changes to the global nitrogen (N) cycle and the effects of atmospheric reactive nitrogen (Nr) deposition on ecosystems have been appreciated for decades but generally assumed to be confined to areas surrounding population centers and restricted to the latter half of the 20th century (*1*–*3*). The result of increasing amounts of Nr in the atmosphere, primarily as NH_3, NO, NO_2, or peroxyacetyl nitrates, is the long-range transport and deposition on continents and oceans as NH_4^+, HNO_3, or NO_3^- (*3, 4*), even in the most remote ecosystems (*5*–*8*). Human activity is therefore generating a new source of atmospheric Nr that is deposited on otherwise pristine ecosystems and could have important effects on primary producers and food webs (*9, 10*).

[1]School of Aquatic and Fishery Sciences, University of Washington, Seattle, WA, USA. [2]St. Croix Watershed Research Station, Science Museum of Minnesota, Marine on St. Croix, MN, USA. [3]Limnology Laboratory, Department of Biology, University of Regina, Regina, Saskatchewan, Canada. [4]Northwest Fisheries Science Center, National Marine Fisheries Service, National Oceanic and Atmospheric Administration, Seattle, WA, USA. [5]Department of Biology, McGill University, Montreal, Quebec, Canada. [6]Key Laboratory of Plateau Lake Ecology and Global Change, School of Tourism and Geography, Yunnan Normal University, Kunming, Yunnan, China. [7]Departments of Geosciences and Biological Sciences, Idaho State University, Pocatello, ID, USA. [8]Department of Earth and Ecosystem Sciences, Division of Geology, Lund University, Sweden. [9]U.S. Fish and Wildlife Service, Togiak National Wildlife Refuge, Dillingham, AK, USA. [10]Mountain Studies Institute, Silverton, CO, USA. [11]Climate Change Institute, University of Maine, Orono, ME, USA. [12]Fisheries and Oceans Canada, Pacific Region, Science Branch, Cultus Lake Salmon Research Laboratory, Cultus Lake, British Columbia, Canada. [13]Department of Earth and Atmospheric Sciences, University of Alberta, Edmonton, Alberta, Canada.

*To whom correspondence should be addressed. E-mail: gholt@uw.edu